Received 17 December 2020; revised 8 April 2021 and 10 May 2021; accepted 12 June 2021.
Date of publication 16 June 2021; date of current version 9 November 2021.

Digital Object Identifier 10.1109/OAJPE.2021.3089678

A New Approach to the Fault Location Problem: Using the Fault's Transient Intermediate Frequency Response

NICOLÁS CIFUENTES (Member, IEEE), and BIKASH C. PAL (Fellow, IEEE)

Department of Electrical and Electronic Engineering, Imperial College, London SW7 2AZ, U.K.

CORRESPONDING AUTHOR: B. C. PAL (b.pal@imperial.ac.uk)

This work was supported by the CONICYT PFCHA/DOCTORADO BECAS CHILE/2017 under Grant 72180289.

ABSTRACT The fault location problem has been tackled mainly through impedance-based techniques, the travelling wave principle and more recently machine learning algorithms. These techniques require both current and voltage measurement. In the case of impedance-based methods they can provide multiples solutions. In the case of the travelling wave approach it usually requires high sampling frequency measurements together with sophisticated identification algorithms. Machine learning techniques require training data and re-tuning for different grid topologies. This paper proposes a new fault location method based on the fault's transient intermediate frequency response of the system immediately after a fault occurs. The transient response is characterized by the travelling wave phenomenon together with intermediate frequencies of oscillation, which are dependent on the faulted section and the fault location. In the proposed fault location solution, an offline methodology identifies these intermediate frequencies and their dependency on the fault location is fitted using a polynomial regression. The online fault location is performed using those polynomial regressions together with voltage measurements from the system and simple signal processing techniques. The full method is tested with an EMT simulation in PSCAD, using the exact frequency dependent model for underground cables.

INDEX TERMS Fault location, frequency-dependent model, PSCAD, state-space model, transient analysis.

NOMENCLATURE

$\mathcal{C}_j$	Set of polynomial coefficients for the intermediate frequencies approximations of the *j-th* cable/line section
$\mathcal{M}_{ij}$	Set of theoretical fault location/intermediate frequencies data points
Ω	Cluster of fault location estimations
τ_i	*i-th* cable/line's traveling delay
$\tilde{K}$	Random variable associated with the theoretical estimated fault location
$\tilde{K}_{est}$	Random variable associated with the estimated fault location
$\tilde{V}_k(\omega)$	Transient voltages' measured frequency response data
$\tilde{W}_i$	Random variable associated with the measured *i-th* intermediate frequency
a_{in}	Coefficients of polynomial approximation for *i-th* intermediate frequency's dependency on the fault location
$H_{mc,i}$	*i-th* cable/line's modal propagation matrix
N_i	Order of polynomial approximation for *i-th* intermediate frequency on the fault location
$p_{k,i}$	Poles of the vector fitting approximations for *i-th* cable/line's constant
$r_{k,i}$	Residues of the vector fitting approximations for *i-th* cable/line's constant
$Y_{m,i}$	*i-th* cable/line's modal exact shunt admittance matrix
$Y_{mc,i}$	*i-th* cable/line's modal characteristic admittance matrix
$Z_{m,i}$	*i-th* cable/line's modal exact series impedance matrix

I. INTRODUCTION

The fault location problem in transmission and distribution systems has been tackled at least since the 70's [1],

and remains an important topic for distribution grid's restoration [2]. Since then, the fault location research field working on centralised algorithmic solutions clustered in three dominant areas [3]–[5]: Impedance-based solutions, Travelling wave approaches and Machine learning algorithms. An extensive review of each methodology is provided in [3]–[5]. Given the ever-evolving and diverse characteristics of current HV and MV networks, fifty years on there is still no universal agreement for a truly applicable and reliable solution. This is evident in the fact that there are currently no centralised fault location methodologies available in transmission or distribution grid protections [3]–[5]. As such, there is still ongoing research to improve each technique into a reliable and applicable methodology [6]–[8].

The first category of impedance-based solutions employs the fundamental frequency behaviour of the grid's currents and voltages during a fault event [3]–[5]. By using RMS measurements of the voltages and currents, it is possible to compute the grid's apparent impedance as seen from the measuring location. If the network's topology is known together with the per-unit impedance of each feeder, then it is possible to define a set of algebraic equations to match the measured impedance to the expected one having the fault location as the unknown variable. The solutions to this set of algebraic equations are thus dependent on the measurement location, the fault location and also the fault impedance [3]–[5]. This approach is limited by two main factors. First, it is necessary to estimate the fault impedance to solve the system of equations. Secondly, depending on the number of available measurements and on their locations, the set of algebraic equations can have multiple fault location solutions [3]–[5], [9].

Regarding travelling wave approaches (also known as transient-based approaches) to the fault location problem, they rely on high-frequency measurements. More specifically, immediately after a fault occurs, pulse-like signals will start propagating from the fault and throughout the system. These pulse waves propagate at a constant speed which is defined by the electrical parameters of the lines and cables, and it is usually around 60% to 90% of the speed of light [3]–[5]. Examples of recent works using this approach can be found in [10]–[12]. On their propagation, each wave will experience reflection and refraction at each discontinuity that they find on lines and cables, creating additional propagating waves. By measuring the travelling time of each pulse-like signal and their respective reflections, it is possible to estimate the fault location from where they started propagating assuming their travelling speed is known [3]–[5]. Due to their high travelling speed, it is necessary to have high sampling frequency devices of at least 100 [kHz] [13], together with synchronized measurements to accurately identify each travelling pulse and to measure their travelling times. This approach has been successfully implemented in the transmission level, for long transmission lines and underground cables. For distribution systems however this approach remains impractical, since it is necessary to distinguish between all the travelling wave signals, which can be cumbersome in real system with several discontinuities [3]–[5] such as LV grids.

Finally, with the advent of machine learning techniques and its growing potential in several fields, some recent research has tried to apply it to the fault location problem. In a similar line of thoughts, new data-driven algorithms have also been developed to tackle the fault-location problem. These algorithms leverage on the wide-area deployment of smart meters in both MV and HV [14]–[16]. In this case, the main drawback is the necessity of having available training data for most machine learning algorithms. In most cases there might not be enough historical data for the training, and synthesizing reliable additional data is most times impractical. Furthermore, the training process needs to be re-tuned for each topological change in the grid [3]–[5].

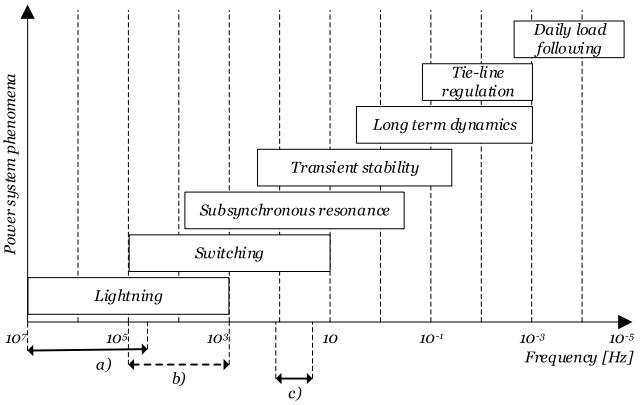

FIGURE 1. Frequency classification for fault location methodologies: a) Travelling wave approaches, b) Intermediate frequencies proposal, c) Impedance-based techniques.

So far, the fault location problem, both in transmission and distribution networks, has been tackled by considering the low or very high frequency behaviour of the system, leaving an unused window of intermediate frequency electromagnetic phenomena as shown in Fig. 1. In just a few cases [17]–[19], the transient behaviour dominated by intermediate frequencies in the range of 5 to 500 kHz as defined in [20] have been used to tackle the problem. For example, in [18], they extend the impedance behaviour approach to frequencies up to 3 kHz to avoid the disturbances created by DGs. In [19], the authors use PMUs data to identify when the zero-sequence current lags the zero-sequence voltage during a fault event to identify the location. This idea is further developed by the authors in [17]. These recent works show that there is an active effort in developing a fault location methodology based on the intermediate frequency transient behaviour of the grid during a fault event.

This paper proposes a new fault location methodology based on the fault's transient intermediate frequency response immediately after a fault event occurs. Instead of extending the impedance analysis approach to higher frequencies, a different direction is taken. A methodology is proposed in

which the intermediate frequencies, present in the transient response of the line/cable system and generated by their natural response, are used to identify the fault location. These intermediate frequencies will be dependent only on the location of where the disturbance occurs, as will be shown in later sections. The main contributions of this work are as follows:

- Demonstrate that a new approach to the fault location problem is possible by considering intermediate frequencies measurement present in the transient response of the system.
- Outline the theoretical foundation for such approach, identifying the key research requirements necessary to identify the system's transient intermediate frequencies and how to use them for solving the fault location problem.
- Propose an offline methodology that characterizes the intermediate frequencies' dependence on the fault location.
- Propose an online fault location methodology which uses the intermediate frequency dependence to identify the fault location. The approach relies on simple signal processing techniques such as the FFT.

The rest of the paper is organized as follows. Section II provides basic theoretical insight on how the intermediate frequencies generated during fault transients depend on the fault location. Section III provides a detailed description of both the offline and online methodologies necessary to identify the fault location. Section IV provides numerical results for a test system using EMT simulations in PSCAD. Conclusions are drawn in Section V.

II. INTUITION

The most basic modelling of a cable/line corresponds to its lumped Π-section representation. This model is valid for low frequencies, where the wavelength of the travelling EM waves is much longer than the length of the line. Although this modelling is not accurate enough for the transient fault location methodology proposed in this work, it provides insight on its theoretical foundation and challenges. During a fault event occurring at a percentage k of the line length D, it is possible to split the original Π-section with parameters R, L and C, into two new sections with scaled electrical parameters as shown in Fig. 2.

$$\ddot{V}_1 + \frac{R}{L}\dot{V}_1 + \frac{2}{k^2LC}V_1 = 0 \tag{1}$$

$$\ddot{V}_2 + \frac{R}{L}\dot{V}_2 + \frac{2}{(1-k)^2LC}V_2 = 0 \tag{2}$$

Considering an ideal fault to ground, i.e. $Z_f = 0$ [Ω], each section will have a transient response defined by the differential equations (1)-(2). The solutions to these equations show that the voltages' $V_1(t)$ and $V_2(t)$ transient response are oscillatory in nature. More importantly, the oscillations have the same damping $\tau = R/L$ but different frequencies ω_1 and ω_2, as defined in their time-domain solutions shown

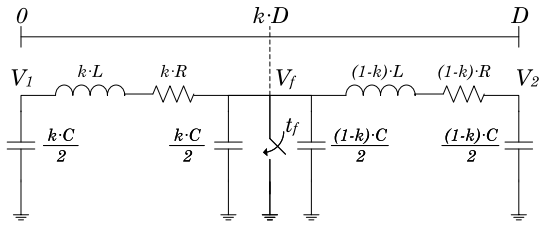

FIGURE 2. Π-section representation of a cable/line during fault event.

in equations (3)-(4).

$$V_1(t) = V_1(t_f) \cdot e^{-\tau t} cos(\omega_1(k) \cdot t + \psi_1(t_f)) \tag{3}$$

$$V_2(t) = V_2(t_f) \cdot e^{-\tau t} cos(\omega_2(k) \cdot t + \psi_2(t_f)) \tag{4}$$

From equations (3)-(4) it is possible to see that the initial conditions $V_1(t_f)$, $V_2(t_f)$, $\phi_1(t_f)$ and $\phi_2(t_f)$ are defined by the fault's occurrence time t_f. The frequency of each transient response however, is dependent exclusively on the fault location according to equations (5)-(6).

$$\omega_1(k) = \sqrt{\frac{2}{LC}} \cdot \frac{1}{k} = \sqrt{\frac{2}{LC}} \sum_{n=0}^{\infty} (-1)^n (k-1)^n \tag{5}$$

$$\omega_2(k) = \sqrt{\frac{2}{LC}} \cdot \frac{1}{1-k} = \sqrt{\frac{2}{LC}} \sum_{n=0}^{\infty} k^n \tag{6}$$

Although equations (5)-(6) are derived in a simplistic scenario, with a single cable section split by an ideal fault, important observations can be made:

1) The intermediate frequencies associated with the transient response of the cable/line system during a fault event are dependent exclusively on the fault location. It is also important to note that, according to equations (5) and (6) the longer the cable/line section is, the lower the associated transient frequency will be. Indeed, if standard L and C parameters are considered, for section lengths ranging from 0.5 to 20 km, their associated transient frequencies will range from around 5 to 500 kHz respectively. Usually this is the normal length of low voltage lines/cables. These frequencies are traditionally associated with switching and lightning electromagnetic phenomena in power system analysis as shown in Fig. 1. To avoid confusion with travelling wave approaches and impedance-based methodologies, this frequency range will be referred in this work as intermediate frequencies, since they correspond to a middle ground between the high and low frequencies used in traditional techniques. The term switching frequency is also avoided since the proposed methodology does not rely on the switching of any specific equipment in the network, but rather on the natural response of the cable/line system to a fault event.
2) In a real system with loads and a non-ideal fault impedance, the different sections will behave

as coupled-oscillators. In addition, the frequency-dependence and distributed behaviour of each section's electrical parameters make it impossible to derive an analytical expressions for the fault location dependence of each frequency $\omega_i(k)$ as the ones in equations (5)-(6). However, a polynomial function $\hat{\omega}_i(k)$ with a sufficiently high order N_i, as defined in equation (7), should be able to accurately represent the fault location dependence of each intermediate frequency $\omega_i(k)$.

$$\omega_i(k) \approx \hat{\omega}_i(k) = \sum_{n=1}^{N_i} a_{in} \cdot k^{n-1} \tag{7}$$

While the previous analysis is intuitive in a deterministic approach, it is necessary for the polynomial approximation to handle frequency measurements as will be explained in the next sections. The intermediate frequency measurements used to solve the fault location problem will contain noise, which needs to be accounted for in the proposed methodology. Thus, it can be assumed that the frequency measurements are random variables which follow a normal distribution of the form $\tilde{W}_i \sim \mathcal{N}(\omega_i(k_r), \sigma_e^2)$ where $\omega_i(k_r)$ is the theoretical frequency corresponding to the real location k_r and σ_e is the measurement error associated with the presence of white noise. In the case of a simple oscillator as the one considered in Fig. 2, the theoretical estimated location is defined by $\tilde{K} = \omega_0/\tilde{W}_1$. Thus, $\tilde{K}$ corresponds to a random variable that doesn't follow a normal distribution as $\tilde{W}_i$ does, but rather as a reciprocal normal distribution which corresponds to a binomial distribution [21]. On the other hand, the estimated location $\tilde{K}_{est}$ is obtained as one of the solutions to the polynomial equation (8) using the measured frequency $\tilde{W}_i$ as will be explained in more detail in the next sections.

$$\tilde{W}_i = \sum_{n=1}^{N_i} a_{in} \tilde{K}_{est}^{n-1} \tag{8}$$

It is thus important that the polynomial regression is performed considering a degree N_i high enough not only to obtain a good deterministic approximation of $\omega_i(k)$, but also so that $\tilde{K}_{est}$ has a probability distribution as close as possible to the reciprocal normal distribution of $\tilde{K}$, to minimize the estimation error of its expected value. An example of the impact that the polynomial regression degree N_i has on the probability density function (pdf) of $\tilde{K}_{est}$ is shown in Fig. 4 when doing a Monte Carlo analysis. More specifically, Fig. 3 and 4 are an example of 10^5 samples of the measured frequency $\tilde{W}$ considering a normal distribution of mean $\mu = 10$ kHz, with a measurement error of $\sigma = 100$ [Hz]. The mean value of 10 kHz corresponds to a fault location of $k = 60$ %, considering an intermediate frequency fault location function $\omega(k) = 2\pi \cdot 6000/k$. In Fig. 4, the binomial distribution of $\tilde{K} = 2\pi \cdot 6000/\tilde{W}$

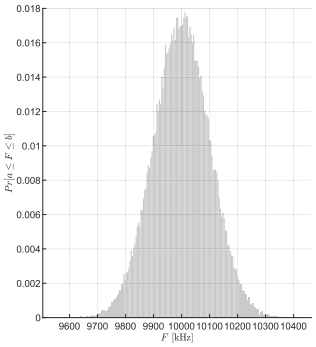

FIGURE 3. Example of random variable $\tilde{F}$. In light grey the histogram of 10^5 samples for $\tilde{F} \sim \mathcal{N}(10^4, 10^6)$.

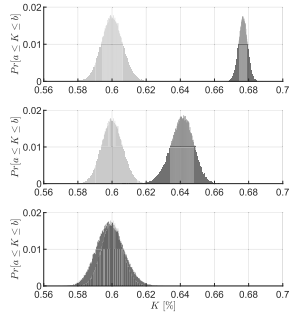

FIGURE 4. Probability density functions in light grey for $\tilde{K}$ and in grey for $\tilde{K}_{calc}$ for 10^5 samples when considering: a) $N_i = 4$, b) $N_i = 7$, c) $N_i = 10$.

is calculated for each sampled point $\tilde{W}$ and shown in light grey. In grey, the distribution of $\tilde{K}_{est}$ is calculated using polynomial approximations of different degrees. From Fig. 4, it is possible to see that low degree approximations are not enough to accurately represent the distribution of $\tilde{K}$. Instead, good approximations of the estimated fault location's binomial distribution can be obtained with a polynomial regression degree of 10 or more.

3) While travelling wave approaches are susceptible to the fault's inception angle, an intermediate frequency methodology wouldn't. More specifically, if the inception angle of the fault is such that the voltage is close enough to zero ($V_f(t_f) \approx 0$), then the travelling signals will have a very small magnitude, comparable to the measurement noise. Intermediate frequencies on the other hand are triggered across the grid and at the time of the fault will not be zero, thanks to the phase angle shift $\psi_i(t_f)$ between voltage signals at different locations in the system.
4) While the previous analysis was performed considering the behaviour of voltage transient signals, an analogous effect occurs for current signals, where their characteristic frequencies of oscillation will depend on the fault location. This means that both voltage and/or current

signals can be used, as opposed to travelling wave approaches and impedance-based techniques were both currents and voltages signals are required. In what follows, the proposed methodology is presented considering voltage measurements, but the same procedures could be done considering current measurements.

From the previous conclusions, the main objectives of the proposed fault location methodology are twofold. First it is necessary to compute the polynomial approximations $\hat{\omega}_{ij}(k)$ describing the fault location dependence of the i^{th} intermediate frequency during a fault in the j^{th} cable section. Secondly, a methodology to estimate the fault location based on the polynomial approximations and real-time measurements needs to be developed. Both methodologies are presented in the next section.

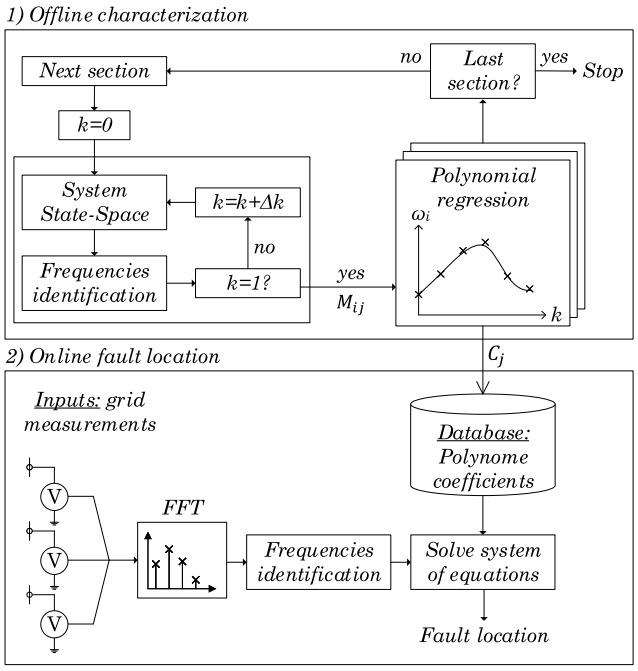

FIGURE 5. Proposed fault-location methodology.

III. FAULT LOCATION METHODOLOGY

The overall intermediate frequency fault location methodology can be divided in two parts, which are applicable to systems with overhead lines, underground cables and hybrid systems. First, an offline methodology is used to obtain the polynomial approximations $\hat{\omega}_{ij}(k)$. This offline characterization stage is simulation-based, by considering the known topology and electrical parameters of the system components. As a result of this stage, each polynomial approximation $\hat{\omega}_{ij}(k)$ can be stored in a database as the set of its polynomial coefficients $\mathcal{C}_{ij} = \{a_{ij1}, \ldots, a_{ijN_{ij}}\}$. The online fault location is then performed on a second stage. This is done by using voltage measurements from the grid, signal processing techniques and the polynomial approximations computed previously. The complete fault location methodology is summarized in Fig. 5. The offline and online stages are described in the next sections.

A. OFFLINE CHARACTERIZATION

The main goal of this stage is to compute the polynomial approximations $\hat{\omega}_{ij}(k)$ of the i^{th} transient response's intermediate frequency during a fault in the j^{th} section of the system. To perform the polynomial approximation it is necessary to have a set of known values $\mathcal{M}_{ij} = \{(k_1, w_{ij}(k_1)), \ldots, (k_{N_d}, w_{ij}(k_{N_d}))\}$, with $0 \leq k_n \leq 1 \; \forall \; n \in \{1, \ldots, N_d\}$. A key aspect for computing these theoretical values is that transient intermediate frequencies are usually found in the 5 to 500 kHz frequency range [20]. In this frequency range, the transient response of the system to a switching event is defined by the frequency-dependent and distributed nature of the cables/lines' electrical parameters. It is thus necessary to consider a model that can accurately represent the cable/lines' behaviour in this frequency range.

The traditional approach to do this would be to use EMT programs such as PSCAD, which can simulate the exact model of cables and lines by using the Universal Line Model (ULM) [22]. By using the waveforms simulated in each fault location scenario, together with signal processing techniques such as the FFT, it would be possible to identify the intermediate frequencies and thus each set $\mathcal{M}_{ij}$. The main drawback to this approach is that the whole process can be time consuming. This can be specially problematic for large systems with short cable/line segments that would require very small time-steps for the simulation exercise.

A different option to simulate the cable's transient response is to consider a linear time invariant (LTI) state-space model approach. From such a model, it is possible to directly derive the system's frequency response to a fault scenario. It is well-known that a line/cable's frequency behaviour is defined by transcendental functions having an infinite number of poles [23], [24]. While such a system is LTI, it is computationally intractable given the requirement to represent a high number of poles to achieve the same accuracy of the ULM over the entire frequency range (up to the [GHz]) commonly considered for the modeling of cable/lines. Some works have intended to tackle this issue by proposing the identification of the system's dominant poles, which have higher observability and impact on the dynamic response during the transient period [23], [24]. More recent approaches have tried to develop an impedance model for cable/lines that is able to capture the frequency-dependent behaviour of their electrical parameters, together with their distributed nature [25], [26]. These methods rely on the rational function approximation of the cable/line's frequency dependent parameters, which can in turn be formulated as an equivalent electrical Π-circuits. In addition, the distributed nature of the electrical parameters gives rise to a travelling delay in its time-domain response, which in these cases is approximated by means of cascading several N Π-circuits obtained by approximating a small fraction l/N of the overall line/cable length l. This last step can significantly increase the order of the impedance model, which limits its applicability in systems with a large number of cable/line sections.

To tackle the LTI modelling in a practical way, the authors use an impedance model for cable/line sections. It is relevant to mention that the accuracy of the proposed fault location methodology is dependent on the state-space model used to represent the system while obtaining the intermediate frequencies polynomial approximations. This however does not invalidate the fault location methodology. On the contrary, it emphasises the need to further develop accurate impedance/LTI models that can complement the ULM analysis done in the time-domain. To be more specific on the modelling of cable/lines being used, the authors consider vector fitting the modal parameters of each cable/line section as follows:

$$Y^{fit}_{mc,i}(s) = d_i + \sum_{k=1}^{N} \frac{r_{k,i}}{s - p_{k,i}} \tag{9}$$

$$H^{fit}_{m,i}(s) = \left(\sum_{k=1}^{\tilde{N}_i} \frac{\tilde{r}_{k,i}}{s - \tilde{p}_{k,i}} \right) e^{-\tau_i s} \tag{10}$$

where $Y^{fit}_{mc,i}(s)$ corresponds to the rational approximation of the cable's modal characteristic impedance $Y_{mc,i}(s)$, and $H^{fit}_{m,i}(s)$ corresponds to the rational approximation of the cable's modal propagation constant $H_{m,i}(s)$. For each modal propagation constant, its associated travelling delay τ_i is extracted as defined in [27]. Each travelling delay can also be approximated by a sum of rational functions of order $N_{d,i}$ by using a Padé approximant. Thus, both $Y^{fit}_{mc,i}(s)$ and $H^{fit}_{m,i}(s)$ can be expressed as a sum of rational functions in the frequency domain. Finally, by combining all the previous rational approximations into the well-known exact Π-section transfer functions, it is possible to obtain a rational approximation for them too as shown in equations (11) and (12). Since the modal travelling delay τ_i is approximated by a Padé approximant, the rational approximations of the impedance transfer functions are accurate up to a critical frequency f_c. In this case, the critical frequency is identified based on a predetermined error threshold σ_e between the theoretical values and the fitted ones as shown in Fig. 6. These critical frequencies will be relevant later on to filter the intermediate frequencies of interest, since they must be accurate enough to use for the fault location problem.

$$Z^{fit}_{m,i}(s) = \frac{Y^{fit}_{mc,i}(s)}{2} \left(\left(H^{fit}_{m,i}(s) \right)^{-1} - H^{fit}_{m,i}(s) \right) \tag{11}$$

$$\frac{Y^{fit}_{m,i}(s)}{2} = Y^{fit}_{mc,i}(s) \left(1 - H^{fit}_{m,i}(s) \right)^{-1} \left(1 + H^{fit}_{m,i}(s) \right) \tag{12}$$

Using this LTI exact Π-circuit impedance representation of each line/cable section, it is possible to define a state-space model for the system in each fault scenario k_n occurring in the j^{th} section as defined in equation (13).

$$\begin{aligned} sX(s) &= A(k_n)X(s) + B(k_n)U(s) \\ V(s) &= D(k_n)X(s) \end{aligned} \tag{13}$$

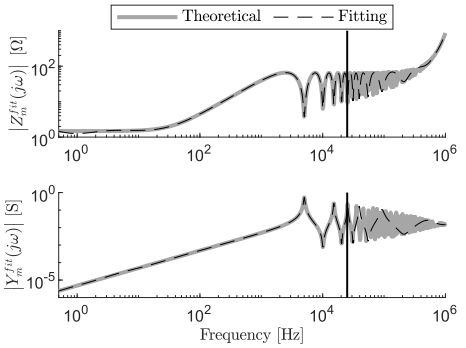

FIGURE 6. **Exact Π-section $Z^{fit}_m(s)$ and $Y^{fit}_m(s)$ approximations examples in the modal domain. The solid grey line represents the theoretical values, the dashed black line the fitted approximation and the solid vertical black line is the critical frequency.**

Once the state-space matrices are determined for a given fault scenario k_n, it is then possible to compute the frequency response of each voltage $V_k(s)$ as defined in equation (14). In equation (14), D_k is the k^{th} row vector from the output matrix $D(k_n)$ while T and Λ correspond to the eigenvalue decomposition matrices of matrix $A(k_n)$ and X_0 are the initial values of the state variables at the time of the fault occurrence. Using equation (14), it is possible to estimate the measured frequency response for each voltage across the network during a fault scenario by computing $V_k(j\tilde{\omega}_i)$. In this case $\tilde{\omega}_i \in \{\tilde{\omega}_1, \ldots, \tilde{\omega}_{NFFT}\}$ corresponds to the set of frequencies available for the FFT computation of the measured voltage waveforms, which are defined by the measuring devices' sampling frequencies and resolutions.

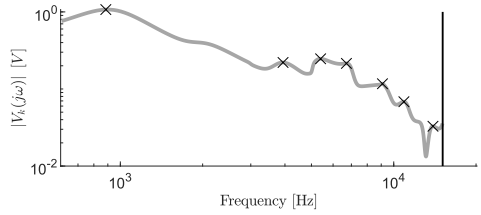

FIGURE 7. **Dominant intermediate frequencies estimated from voltage's frequency response.**

Once the frequency response $V_k(j\omega)$ has been computed, the dominant intermediate frequencies of the transient response can be estimated. For each voltage measurement waveform $V_k(t)$, its dominant intermediate frequencies are defined in this work as the ones associated with the peak values of its frequency response's magnitude $|V_k(j\omega)|$ as shown in Fig. 7. Only the peak values below the critical frequencies f_c should be considered to ensure good accuracy in accordance with the rational approximations of the line/cables impedance behaviour. An example of the upper bound f_c is shown with a solid black line in Fig. 7. It is also important to consider the dominant frequencies above the fundamental frequency f_0 and some of its harmonics, since

those frequencies don't correspond to the transient response of the cable system but rather with its forced response.

$$V_k(s) = D_k T^{-1} (sI - \Lambda)^{-1} T (X_0 + BU(s)) \qquad (14)$$

The set of theoretical dominant intermediate frequencies $\mathcal{M}_{ij} = \{(k_1, w_{ij}(k_1)), \ldots, (k_{N_d}, w_{ij}(k_{N_d}))\}$ can then be constructed by iteratively extracting the frequency response's peak values for each fault scenario k_n using the state-space representation from eq. (13). The number of theoretical values is defined by the section's length partitioning according to Δk. Thus, Δk must be selected to have enough data points to achieve the desired polynomial regression accuracy while keeping a reasonable computation time of the offline methodology. More data points allow to perform higher order polynomial regressions with better accuracy at the cost of more computation time. In the authors' experience, good results can be achieved by considering 10 to 15 data points, i.e. a step of $\Delta k \in [0.0714, 0.1]$ for each cable section.

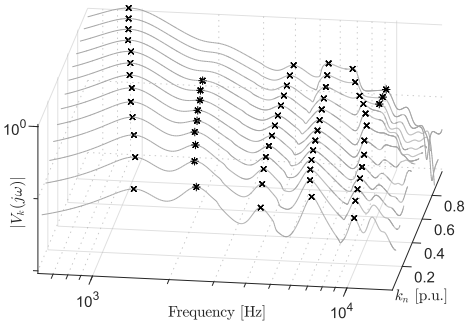

FIGURE 8. Dominant intermediate frequencies tracking over different fault location scenarios on the same cable/line section.

One last point to consider in this process is that not all intermediate frequencies correspond to peak values of the voltages' frequency responses across all fault scenarios k_n. This is represented in the example shown in Fig. 8, where the black crosses correspond to intermediate frequencies that consistently represent peak values of the voltage's frequency response for all fault location scenarios k_n. The black stars on the other hand correspond to intermediate frequencies that represent peak values in some fault location cases, but not in all of them. These intermediate frequencies must thus be identified and filtered out after computing the peak values for all fault scenarios k_n within the j^{th} cable/line section.

Finally, once the set $\mathcal{M}_{ij}$ is computed, each intermediate frequency fault location dependency $\omega_{ij}(k)$ can be fitted using a polynomial regression $\hat{\omega}_{ij}(k)$. Each polynomial fitting can be stored as the set of its coefficients $\mathcal{C}_{ij} = \{a_{ij1}, \ldots, a_{ijN_{ij}}\}$, where N_{ij} is the order of each polynomial regression. These coefficients are the main outcome of the offline characterization methodology in order to solve the fault location problem, as it is explained in the next section. The coefficients can be further grouped for the j^{th} section as $\mathcal{C}_j = \{\mathcal{C}_{1j}, \ldots, \mathcal{C}_{Nj}\}$.

This offline methodology must be performed for each topology of interest. This in turn means that the offline methodology should be updated each time a topological change is performed, i.e. new lines, loads or generators are connected to the grid. Despite of this, the proposed offline methodology has two advantages in comparison with other simulation-based approaches. Firstly, the offline characterization can be performed for each cable/line section independently, which means it could be performed in parallel, greatly reducing computational time and improving its scalabilty for larger systems. Secondly, simulation-based methods that match time-domain simulations with field measurements must consider different fault inception angle conditions. The proposed offline methodology relies only in the intermediate frequency of oscillations during the transient response of the system and thus doesn't need to consider different fault inception angle conditions. Further research can be done to optimize the proposed offline methodology, for example by applying model order reduction techniques to make the LTI representation of the system, making it more tractable without compromising its accuracy.

B. ONLINE FAULT LOCATION

The offline characterization methodology is designed to tackle most of the modelling and analysis complexity to solve the fault location problem. This in turn allows the online fault location method to remain simple in its implementation and applicability.

The first step to perform the real-time fault location is to obtain the time-domain waveforms of the transient voltages $\tilde{V}_k(t)$ generated immediately after the occurrence of a fault in the system. Using traditional FFT techniques, together with the necessary windowing and filtering processes to discard high-frequency noise and to avoid spectral leakage, the measured frequency response $\tilde{V}_k(j\omega)$ for each measured voltage waveform is computed.

In a second step, the measured dominant intermediate frequencies $\tilde{\omega}_i$ for each transient measurement are identify using the same peak-value identification process used in the offline characterization methodology. In this case, the search for the peak values is performed in the magnitude of the measured frequency response $\left|\tilde{V}_k(j\omega)\right|$. It is worth mentioning that each intermediate frequency $\tilde{\omega}_i$ won't be observable in all measured voltage waveforms $\tilde{V}_k(t)$. The set of intermediate frequencies can be obtained from the eigenvalues of matrix A from the state-space representation in eq. (13). The dominant intermediate frequencies in each voltage waveform $\tilde{V}_k(t)$ depend, however, on their respective participations to each voltage's transient response. The participation of each intermediate frequency in the k^{th} voltage waveform will thus depend on its associated residue coefficient. The residues coefficients can be computed from the eigenvector matrix T together with the respective k^{th} row vector of the output matrix D [28]. In order to have full observability of all dominant intermediate frequencies $\tilde{\omega}_i$, an optimization problem can be defined to establish the optimal allocation of the measuring devices in the grid across a set of credible

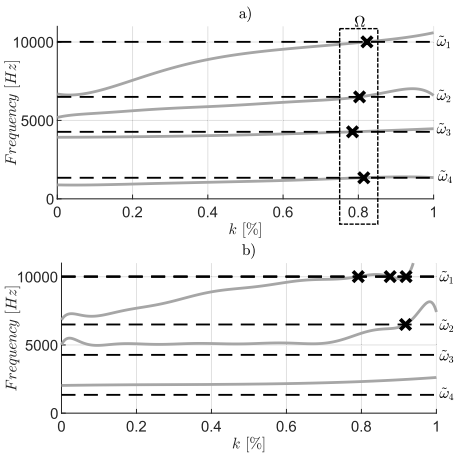

FIGURE 9. Example of polynomial solutions for set of measured frequencies $\tilde{\omega}_i$: a) Equations obtained for scenario of faulted section, b) Equations obtained for scenario of non-faulted section.

and/or critical fault location scenarios. This problem however is not tackled in this work and remains open for future research. In what follows of the online methodology, it is assumed that enough measurement devices are available to identify the dominant intermediate frequencies.

Once the dominant intermediate frequencies $\tilde{\omega}_i$ have been identified, they can be used to solve the fault location problem. This is done by identifying the faulted section and the fault location $\hat{k}$ within said section. This can be done by solving the system of polynomial equations $\mathcal{C}_j$ obtained while considering a fault occurring in each j^{th} section as defined in eq. (15). In this case, if the j^{th} section has N_j set of polynomial equations $\hat{\omega}_i(k)$, and there are N_f measured dominant intermediate frequencies $\tilde{\omega}_i$, then there is a total of $N_j \times N_f$ equations to solve. When the polynomial regressions being solved are the ones that were obtained for a fault scenario that simulated the actual faulted section, then there will be a cluster $\Omega = \left\{\tilde{k}_1, \ldots, \tilde{k}_{N_f}\right\}$ of fault location estimates around the value of the real fault location $\hat{k}$. Such a cluster will not exist when considering the polynomial regressions obtained for fault scenarios simulated in other cable/line sections. While this might not be obvious from eq. (15), an example is provided in Fig. 9. In the example, a set of four measured dominant intermediate frequencies $\tilde{\omega}_i$ are considered. When solving the polynomial regressions obtained when simulating the actual faulted section there is a cluster of solutions around the real fault location value. This is not the case when considering the polynomial equations associated with a different faulted section scenario, where multiple estimates of the location do not provide a clear cluster.

$$\begin{aligned}
\hat{\omega}_1(k) &= a_{11} + \ldots + a_{1N_1}k^{N_1-1} = \tilde{\omega}_1 \\
&\vdots \\
\hat{\omega}_1(k) &= a_{11} + \ldots + a_{1N_1}k^{N_1-1} = \tilde{\omega}_{N_f} \\
&\vdots \\
\hat{\omega}_{N_j}(k) &= a_{N_j1} + \ldots + a_{N_jM}k^{M-1} = \tilde{\omega}_1 \\
&\vdots \\
\hat{\omega}_{N_j}(k) &= a_{N_j1} + \ldots + a_{N_jM}k^{M-1} = \tilde{\omega}_{N_f}
\end{aligned} \tag{15}$$

The online fault location can thus be performed by solving the set of polynomial regressions of each cable/line section using the measured intermediate frequencies until a cluster of solutions is found. The cluster of solutions should be defined by finding at least one solution per polynomial regression, and having all the solutions within a maximum distance deviation threshold Δk_j predefined beforehand. In the next section, numerical results are provided when the methodology is tested using EMT cable models in PSCAD.

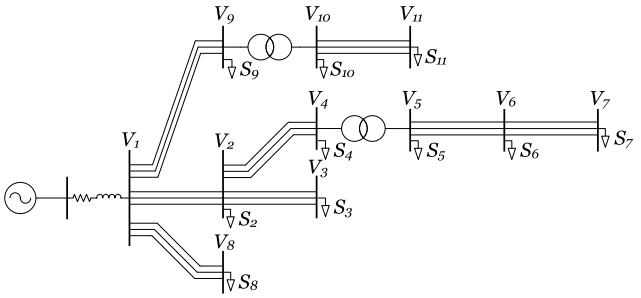

FIGURE 10. PSCAD cable test system.

TABLE 1. Cable data.

Parameters	Value
Configuration	Three cables flat
Cable separation	0.5 [m]
Cable depth	1 [m]
Rated line to line voltage	11 [kV]
Conductor outer radius	0.0047 [m]
Conductor material: copper	$\rho_{cu} = 172.4$ [$\mu\Omega$·m]
1st insulating layer thickness	0.0034 [m]
1st insulating layer material: XLPE	$\epsilon_1 = 2.5$
Sheath thickness	0.0019 [m]
Sheath material: copper	$\rho_{cu} = 172.4$ [$\mu\Omega$·m]
2nd insulating layer thickness	0.0018 [m]
2nd insulating layer material: PVC	$\epsilon_2 = 8$

IV. NUMERICAL RESULTS

To test the proposed fault location methodology, a 11 kV three-phase cable test system was built in PSCAD, as shown in Fig. 10. The cable model used for the time-domain simulations is the *Frequency Dependent (Phase) Model*, which implements the ULM scheme. The cable's characteristics are summarized in Table 1, and the system parameters are presented in Table 2. Two transformers are modelled using their T-models, i.e. a shunt branch to represent their magnetizing properties and two series branches two account for the leakage reactances and resistances. Loads are represented using realistic dynamic ERLM models as defined in [29].

TABLE 2. System data.

Parameters	Value
Header equivalent resistance	$R_{tf} = 1\ [\Omega]$
Header equivalent inductance	$L_{tf} = 0.1\ [H]$
Cable 1-2 length	5.0 [km]
Cable 2-3 length	6.0 [km]
Cable 2-4 length	2.0 [km]
Cable 5-6 length	3.0 [km]
Cable 6-7 length	2.0 [km]
Cable 1-8 length	20.0 [km]
Cable 1-9 length	2.0 [km]
Cable 10-11 length	5.0[km]
Transformer 4-5 rated power	0.2 [MVA]
Transformer 4-5 leakage reactances	$X_1 = X_2 = 0.1\ [pu]$
Transformer 4-5 leakage resistances	$R_1 = R_2 = 0.05\ [pu]$
Transformer 4-5 magnetizing reactance	$X_m = 500\ [pu]$
Transformer 4-5 magnetizing resistance	$R_m = 500\ [pu]$
Transformer 9-10 rated power	0.1 [MVA]
Transformer 9-10 leakage reactances	$X_1 = X_2 = 0.1\ [pu]$
Transformer 9-10 leakage resistances	$R_1 = R_2 = 0.05\ [pu]$
Transformer 9-10 magnetizing reactance	$X_m = 500\ [pu]$
Transformer 9-10 magnetizing resistance	$R_m = 500\ [pu]$

More specifically, each load's dynamic behaviour is defined in PSCAD by equations (16) and (17), where all loads have the same paramaters $\alpha_s = 0.38$, $\alpha_t = 2.26$, $T_{pr} = 2.26\ [s]$, $\beta_s = 2.68$, $\beta_t = 5.22$ and $T_{qr} = 70\ [s]$ according to [29].

$$\begin{aligned} \dot{P}_r + T_{pr}P_r &= P_s - P_t \\ P &= P_r + P_{tr} \\ P_s(V) &= P_0\left(\frac{V}{V0}\right)^{\alpha_s} \\ P_t(V) &= P_0\left(\frac{V}{V0}\right)^{\alpha_t} \end{aligned} \tag{16}$$

$$\begin{aligned} \dot{Q}_r + T_{qr}Q_r &= Q_s - Q_t \\ Q &= Q_r + Q_{tr} \\ Q_s(V) &= Q_0\left(\frac{V}{V0}\right)^{\beta_s} \\ Q_t(V) &= Q_0\left(\frac{V}{V0}\right)^{\beta_t} \end{aligned} \tag{17}$$

From equations (16) and (17), it is possible to obtain the time-domain behaviour of loads immediately after the occurrence of a fault at time t_f as defined by equations (18) [29], where a voltage drop occurs from from the steady-state value V_s to the fault value V_f.

$$\begin{aligned} P(t) &= P_s(V_f) + \left[\Delta P(V_s) - \Delta P(V_f)\right] e^{\frac{-(t-t_f)}{T_{pr}}} \\ Q(t) &= Q_s(V_f) + \left[\Delta Q(V_s) - \Delta Q(V_f)\right] e^{\frac{-(t-t_f)}{T_{qr}}} \\ \Delta P(V) &= P_s(V) - P_t(V) \\ \Delta Q(V) &= Q_s(V) - Q_t(V) \end{aligned} \tag{18}$$

To represent the load behaviour in the LTI representation of the grid in the offline characterization, two key aspects need to be considered:

- The time response of the loads is much slower than the transient response of the cable/line system. The transient behaviour of the intermediate frequencies occurs within the [μs] range, while the load dynamics is in the [s] range which means that $e^{\frac{-(t-t_f)}{T_{pr}}} \approx 1$.
- The voltage drop from V_s to V_f is not instantaneous. While this is the case in RMS simulation, in the EMT case the rate of change of voltages across the grid is limited by the grid's dynamics, i.e. it's inductances and capacitances. More importantly, immediately after the fault occurrence and during the first [μs] when the intermediate frequencies' transient behaviour is dominating, it can be considered that $V_f \approx V_s \Rightarrow \Delta P(V_s) \approx \Delta P(V_f)$.

With the previous two considerations, for the purposes of the offline characterization the loads can be considered as static and defined by equations (19), where the steady-state voltages V_s can be computed from the load-flow solutions for the grid on a given operating condition. In general, these values will be constrained to a narrow operational band around 1.0 pu as defined by each country's grid code.

$$\begin{aligned} P(t) = P_s(V_s) \Rightarrow R &= \frac{V_s^2}{P_s(V_s)} \\ Q(t) = Q_s(V_s) \Rightarrow X &= \frac{V_s^2}{Q_s(V_s)} \end{aligned} \tag{19}$$

The time-domain simulations are performed in PSCAD considering a the time-step of $\epsilon = 2\ [\mu s]$ and a sampling frequency of 30 [kHz]. The offline characterization of a single cable section takes approximately 23 [min] in a Intel Core i7-10750 CPU of 2.6 [GHz], with a total RAM usage of 2.4 [GB]. While this time and memory consumption can be improved with code optimization, from a theoretical perspective the computational burden comes from the matrices' size of the LTI state-space representation of the system. To improve the scalability of the proposed methodology to bigger systems, future works needs to be done to reduce the order of the LTI models while preserving its accuracy for the purposes of the offline characterization.

To test the proposed fault location methodology, three fault scenarios are considered:

1) Scenario 1: three-phase fault with $R_f = 0.2\ [\Omega]$ at 30% of cable 2-3
2) Scenario 2: three-phase fault with $R_f = 2\ [\Omega]$ at 80% of cable 1-2
3) Scenario 3: three-phase fault with $R_f = 20\ [\Omega]$ at 50% of cable 5-6

For each fault scenario, the transient voltage waveforms are recorded and then processed in Matlab. A blackman windowing is applied to the sampled signals and the FFT is computed. Since the modelling of the cable system is done in the modal domain using the state-space representation described in Section III-A, the voltage waveforms are

TABLE 3. Load data.

Load	P_0 [MW]	Q_0 [MVAr]	$V_s[pu]$
S_2	0.05	0.1	0.97
S_3	0.03	0.15	0.97
S_4	0.05	0.015	0.97
S_5	0.15	0.07	0.945
S_6	0.015	0.015	0.945
S_7	0.015	0.015	0.945
S_8	0.15	0.07	0.972
S_9	0.01	0.02	0.975
S_{10}	0.07	0.03	0.974
S_{11}	0.03	0.015	0.973

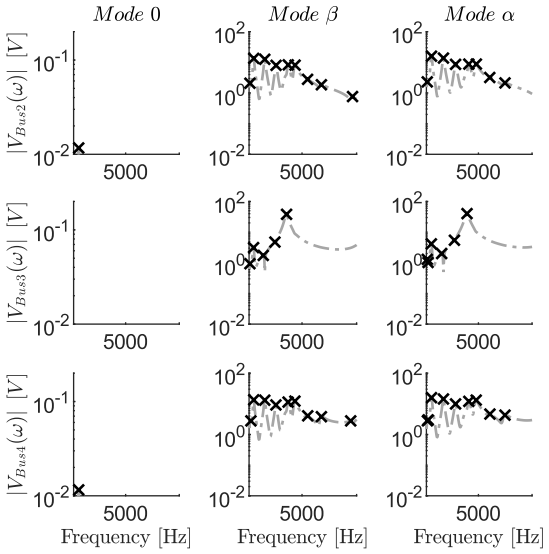

FIGURE 11. Frequency spectrum of voltages' transient response during fault scenario 1.

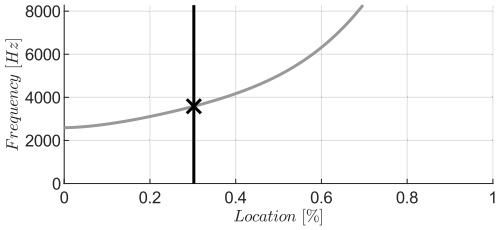

FIGURE 12. Fault location solution for fault scenario 1 using Bus 3 polynomial regressions.

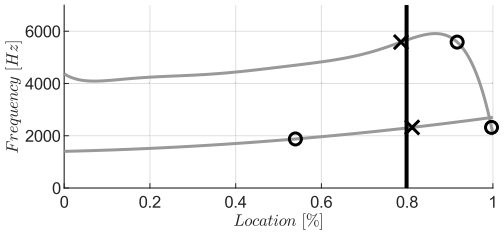

FIGURE 13. Fault location solution for fault scenario 2 using Bus 2 polynomial regressions.

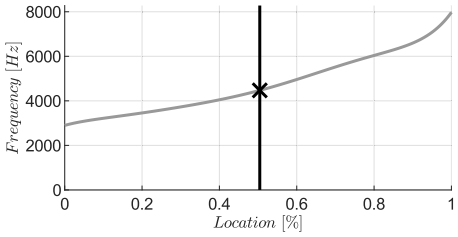

FIGURE 14. Fault location solution for fault scenario 3 using Bus 6 polynomial regressions.

transformed to the modal domain using the Clarke transform to be consistent in the analysis. The dominant intermediate frequencies are tracked by identifying the peak values of the frequency responses' magnitude, in a range of frequencies below the critical fitting frequencies f_c computed in the offline characterization of the cable system. An example of the process' outcome is shown in Fig. 11 for voltage measurements performed in busbars 2, 3 and 4 during fault scenario 1.

The results of the fault location estimations are shown from Fig. 12 to 14 respectively. In all cases the faulted section is identified with either the existence of a single solution or a cluster of solutions around the real fault location value. In addition, the average of the fault location estimates $\tilde{k}_i$ is shown with a solid black line.

As it is possible to see from Fig. 12 to 14, the final fault location estimation using the average of the found solutions is very close to the actual values. More specifically, in the fault scenario 1 where the fault occurs at 30% of cable 23, the estimated fault location is 30.24%, which translates in a final error of 0.8% or 48 m. In fault scenario 2, the final estimation is 79.86%, which translates in a final error of 0.18% or 8.75 m. Finally, for the fault scenario 3, the final estimation is 50.44%, which translates in a final error of 0.88% or 26.4 m. In fault scenario 2, three outsider solutions are also identified, marked by circles in Fig. 13, and discarded since they don't belong to any cluster of solutions.

To test the validity of the proposed methodology in longer cable/line sections, two additional fault scenarios are performed in cable 1-8 with a length of 20 km:

- Scenario 4: three-phase fault with $R_f = 0.2$ [Ω] at 25% of cable 1-8
- Scenario 5: three-phase fault with $R_f = 0.2$ [Ω] at 50% of cable 1-8

The fault location results for fault scenarios 4 and 5 are shown in Fig. 16 and 17 respectively, where the fault estimation is performed considering the polynomial equations of bus 1. When performing the proposed methodology to faults occurring in cable 1-8, the methodology can provide accurate results. More specifically, by using the frequencies measured at bus 1, the methodology is able to correctly identify the first

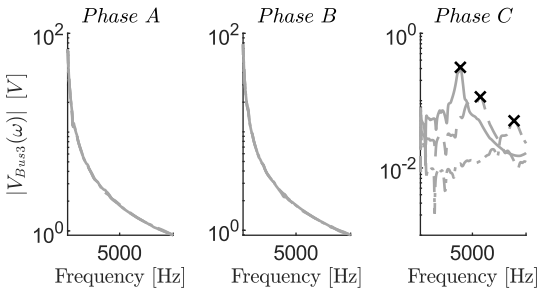

FIGURE 15. Frequency spectrum of voltages' transient response for a fault inception angle of zero in cable 23. The solid line if for a fault at 30%, the dashed line for 50% and the dotted line for 70%.

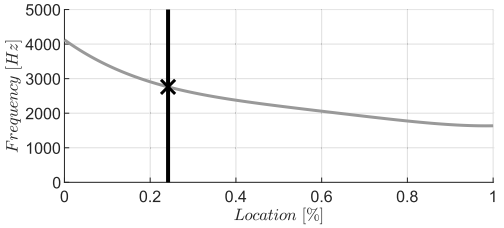

FIGURE 16. Fault location solution for fault scenario 4 using Bus 1 polynomial regressions.

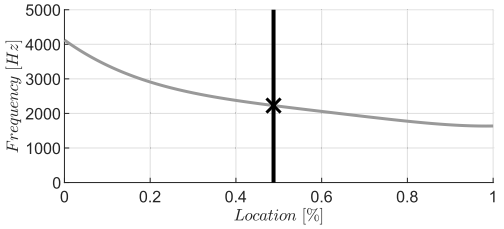

FIGURE 17. Fault location solution for fault scenario 5 using Bus 1 polynomial regressions.

fault at 24.17% of the cable with a precision of 3.3% or 166 m. The second fault is estimated to occur at 48.77%, equivalent to a 2.46% error or 246 m.

Finally, a single phase to ground fault with a fault inception angle of zero is simulated in cable 23. The frequency spectrum of the phase voltages at Bus 3 are shown in Fig. 15, for different fault locations. For the proposed offline methodology to emulate unbalanced faults and apply the fault location methodology, the current LTI impedance modelling defined in equations (12) and (11) needs to be extended from the modal to the phase domain. That being said, from Fig. 15 it is possible to see that there are intermediate frequencies that depend on the fault location present in the faulted phase C, more specifically the one with values 3875, 5737 and 8880 Hz. This intermediate frequency could be used to solve the fault location using the proposed fault location methodology considering the extended phase domain impedance modelling of cable/lines, which remains an open research challenge for future works. This again reinforces the need for further research on the impedance modelling of cables/lines to complement EMTP time-domain simulations with frequency-domain analysis.

V. CONCLUSION

In this paper, a novel fault location methodology is proposed for cable/line systems. The methodology relies on the system's transient response immediately after a fault occurs. More importantly, the natural frequencies of oscillations generated by the fault event are dependent on the faulted section and the fault location within that section.

On a first step, the cable/line system is modelled using an LTI representation from which the intermediate frequencies of oscillation present in the transient response can be identified. Once this process is performed for various fault location scenarios in a given cable/line section, a polynomial regression can be used to characterize the fault location dependency of the system's transient intermediate frequencies. The process is thus repeated for all sections in the systems. The online fault location problem can thus be solved using simple signal processing techniques such as the FFT on the measured waveforms of the system's transient response. In addition, the methodology is able to identify the faulted section in the system, which avoids the problem of multiples fault location estimations.

The methodology proved to be efficient in a test case simulated in an EMT software like PSCAD, while using an exact frequency-dependent model for underground cables, realistic load models and transformers. As such, it is proven that the transient behaviour of the system can be efficiently used to solve the fault location problem, without the drawbacks of other available techniques. As a new approach to the fault location problem, there are still some challenges to tackle to improve the proposed technique. Further research can be performed in order to improve the LTI representation of the cable/line system which has a direct impact on the accuracy of the proposed method.

REFERENCES

[1] B. Clegg and N. G. Lord, "Modern cable-fault-location methods," *Proc. Inst. Electr. Engineers*, vol. 122, no. 4, pp. 395–402, 1975.

[2] F. Shen, Q. Wu, and Y. Xue, "Review of service restoration for distribution networks," *J. Modern Power Syst. Clean Energy*, vol. 8, no. 1, pp. 1–14, 2020.

[3] A. Farughian, L. Kumpulainen, and K. Kauhaniemi, "Review of methodologies for Earth fault indication and location in compensated and unearthed MV distribution networks," *Electr. Power Syst. Res.*, vol. 154, pp. 373–380, Jan. 2018.

[4] A. Bahmanyar, S. Jamali, A. Estebsari, and E. Bompard, "A comparison framework for distribution system outage and fault location methods," *Electr. Power Syst. Res.*, vol. 145, pp. 19–34, Apr. 2017.

[5] S. S. Gururajapathy, H. Mokhlis, and H. A. Illias, "Fault location and detection techniques in power distribution systems with distributed generation: A review," *Renew. Sustain. Energy Rev.*, vol. 74, pp. 949–958, Jul. 2017.

[6] F. Zhang, Q. Liu, Y. Liu, N. Tong, S. Chen, and C. Zhang, "Novel fault location method for power systems based on attention mechanism and double structure GRU neural network," *IEEE Access*, vol. 8, pp. 75237–75248, 2020.

[7] D. Guillen, C. Salas, L. F. Sanchez-Gomez, and L. M. Castro, "Enhancement of dynamic phasor estimation-based fault location algorithms for AC transmission lines," *IET Gener., Transmiss. Distrib.*, vol. 14, no. 6, pp. 1091–1103, Mar. 2020.

[8] L. Xie, L. Luo, Y. Li, Y. Zhang, and Y. Cao, "A traveling wave-based fault location method employing VMD-TEO for distribution network," *IEEE Trans. Power Del.*, vol. 35, no. 4, pp. 1987–1998, Aug. 2020.
[9] K. Zhang, Y. Zhu, and X. Liu, "A fault locating method for multi-branch hybrid transmission lines in wind farm based on redundancy parameter estimation," *J. Modern Power Syst. Clean Energy*, vol. 7, no. 5, pp. 1033–1043, Sep. 2019.
[10] R. Liang *et al.*, "Fault location method in power network by applying accurate information of arrival time differences of modal traveling waves," *IEEE Trans. Ind. Informat.*, vol. 16, no. 5, pp. 3124–3132, May 2020.
[11] S. Shi, B. Zhu, A. Lei, and X. Dong, "Fault location for radial distribution network via topology and reclosure-generating traveling waves," *IEEE Trans. Smart Grid*, vol. 10, no. 6, pp. 6404–6413, Nov. 2019.
[12] Y. Xi, Y. Cui, X. Tang, Z. Li, and X. Zeng, "Fault location of lightning strikes using residual analysis based on an adaptive Kalman filter," *IEEE Access*, vol. 7, pp. 88126–88137, 2019.
[13] A. Ahmadimanesh and S. M. Shahrtash, "Transient-based fault-location method for multiterminal lines employing S-transform," *IEEE Trans. Power Del.*, vol. 28, no. 3, pp. 1373–1380, Jul. 2013.
[14] Y. Jiang, "Data-driven fault location of electric power distribution systems with distributed generation," *IEEE Trans. Smart Grid*, vol. 11, no. 1, pp. 129–137, Jan. 2020.
[15] K. Chen, J. Hu, Y. Zhang, Z. Yu, and J. He, "Fault location in power distribution systems via deep graph convolutional networks," *IEEE J. Sel. Areas Commun.*, vol. 38, no. 1, pp. 119–131, Jan. 2020.
[16] W. Li, D. Deka, M. Chertkov, and M. Wang, "Real-time faulted line localization and PMU placement in power systems through convolutional neural networks," *IEEE Trans. Power Syst.*, vol. 34, no. 6, pp. 4640–4651, Nov. 2019.
[17] X. Wang *et al.*, "Location of single phase to ground faults in distribution networks based on synchronous transients energy analysis," *IEEE Trans. Smart Grid*, vol. 11, no. 1, pp. 774–785, Jan. 2020.
[18] K. Jia, T. Bi, Z. Ren, D. W. P. Thomas, and M. Sumner, "High frequency impedance based fault location in distribution system with DGs," *IEEE Trans. Smart Grid*, vol. 9, no. 2, pp. 807–816, Mar. 2018.
[19] X. Wang, H. Zhang, F. Shi, W. Xie, P. Ling, and J. Liu, "Transient energy analysis based single-phase-to-ground fault location in distribution networks," in *Proc. 2nd IEEE Conf. Energy Internet Energy Syst. Integr. (EI2)*, Oct. 2018, pp. 1–4.
[20] *IEEE Recommended Practice for Monitoring Electric Power Quality*, Standard 1159-2019 (Revision IEEE Std 1159-2009), 2019, pp. 1–98, 2019.
[21] N. L. Johnson, "Continuous univariate distributions," in *Wiley Series in Probability and Mathematical Statistics Applied Probability and Statistics*, 2nd ed. New York, NY, USA: Wiley, 1994.
[22] A. Morched, B. Gustavsen, and M. Tartibi, "A universal model for accurate calculation of electromagnetic transients on overhead lines and underground cables," *IEEE Trans. Power Del.*, vol. 14, no. 3, pp. 1032–1038, Jul. 1999.
[23] S. L. Varricchio, F. D. Freitas, N. Martins, and F. C. Veliz, "Computation of dominant poles and residue matrices for multivariable transfer functions of infinite power system models," *IEEE Trans. Power Syst.*, vol. 30, no. 3, pp. 1131–1142, May 2015.
[24] N. Martins, C. Portela, and S. Gomes, "Sequential computation of transfer function dominant poles of s-domain system models," *IEEE Trans. Power Syst.*, vol. 24, no. 2, pp. 776–784, May 2009.
[25] P. T. Caballero, S. Kurokawa, and B. Kordi, "Accelerated frequency-dependent method of characteristics for the simulation of multiconductor transmission lines in the time domain," *Electr. Power Syst. Res.*, vol. 168, pp. 55–66, Mar. 2019.
[26] A. Hoshmeh, "A three-phase cable model based on lumped parameters for transient calculations in the time domain," in *Proc. IEEE Innov. Smart Grid Technol. Asia (ISGT–Asia)*, Nov. 2016, pp. 580–585.
[27] B. Gustavsen, "Optimal time delay extraction for transmission line modeling," *IEEE Trans. Power Del.*, vol. 32, no. 1, pp. 45–54, Feb. 2017.
[28] J. Rommes and N. Martins, "Efficient computation of multivariable transfer function dominant poles using subspace acceleration," *IEEE Trans. Power Syst.*, vol. 21, no. 4, pp. 1471–1483, Nov. 2006.
[29] D. Karlsson and D. J. Hill, "Modelling and identification of nonlinear dynamic loads in power systems," *IEEE Trans. Power Syst.*, vol. 9, no. 1, pp. 157–166, Feb. 1994.

NICOLÁS CIFUENTES (Member, IEEE) was born in Santiago, Chile. He received the B.S. and M.S. degrees in electrical engineering from the University of Chile, Santiago, in 2017. He is currently pursuing the Ph.D. degree with the Control and Power Group, Department of Electrical and Electronic Engineering, Imperial College London. His main interests include power systems' dynamic modeling, control and stability, dynamic impact and control strategies in large-scale integration of converter-based technologies for power generation, and FACT devices.

BIKASH C. PAL (Fellow, IEEE) received the B.E.E. (Hons.) degree from Jadavpur University, Calcutta, India, in 1990, the M.E. degree from the Indian Institute of Science, Bengaluru, India, in 1992, and the Ph.D. degree from the Imperial College London, London, U.K., in 1999, all in electrical engineering. He is currently a Professor with the Department of Electrical and Electronic Engineering, Imperial College London. His current research interests include renewable energy modeling and control, state estimation, and power system dynamics. He is the Vice President of the IEEE Power and Energy Society. He is a Fellow of IEEE for his contribution to power system stability and control. He was the Editor-in-Chief of the IEEE TRANSACTIONS ON SUSTAINABLE ENERGY from 2012 to 2017 and *IET Generation, Transmission and Distribution* from 2005 to 2012.